Materials Science & Engineering A 939 (2025) 148479

Contents lists available at ScienceDirect

Materials Science & Engineering A

journal homepage: www.elsevier.com/locate/msea

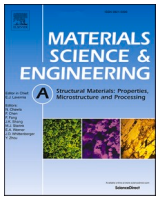

Enhanced crack stability in micro scale fracture testing via optimized bridge notches

Eloho Okotete [a], Alban Muslija [b,c], Judith K. Hohmann [b,c], Manfred Kohl [b,c], Steffen Brinckmann [d], Subin Lee [a,*], Christoph Kirchlechner [a]

[a] Institute for Applied Materials, Karlsruhe Institute of Technology, D-76344, Eggenstein-Leopoldshafen, Germany
[b] Institute of Microstructure Technology, Karlsruhe Institute of Technology, D-76344, Eggenstein-Leopoldshafen, Germany
[c] Karlsruhe Nano Micro Facility (KNMFi), Karlsruhe Institute of Technology, D-76344, Eggenstein-Leopoldshafen, Germany
[d] Structure and Function of Materials, Forschungszentrum Jülich GmbH, D-52428, Jülich, Germany

ARTICLE INFO

Keywords:
Bridge notch
Notch geometry
Micro cantilever
Fracture toughness
FIB artefact
Silicon

ABSTRACT

In micro cantilever fracture, a bridge notch geometry with material ligaments at the notch ends helps to reduce focused ion beam artefacts near the notch root by arresting initial cracks and promoting fracture from sharp, natural cracks. Thus, it significantly reduces the statistical scatter in fracture toughness, a common but undesirable feature in micro fracture testing. Although this concept has been validated in simulations and experiments, systematic investigations into the optimal geometry remain lacking. In this study, we experimentally examine the influence of bridge width and notch depth on the fracture toughness of micro cantilevers, using single crystalline silicon as a model material. We found that samples with thinner material bridges and deeper notches exhibit crack arrest before failure, while those with thicker bridges do not show crack arrest instead exhibit apparent toughening. Cantilevers with an optimized bridge notch geometry for crack arrest exhibit a K_{IC} of 1.09 ± 0.02 MPa $m^{0.5}$, which agrees with previously reported fracture toughness for the Si (111) surface. Additionally, discrepancies between the bridge geometry in the experiment and the ideal structure resulted in a mismatch between the predicted and observed notch requirements for crack arrest. Our findings offer practical guidelines for designing bridge notch geometries to promote bridge failure, thus improving statistical analysis in micro fracture.

1. Introduction

Fracture toughness measurements at small length scales are now possible for various material systems from hard coatings to thin films, facilitated by mostly specialized indentation-based methods. These include traditional experimental approaches that estimate toughness from crack lengths generated around residual indents [1,2], as well as more advanced techniques such as single cantilever beam fracture, double cantilever beam fracture, and micro pillar splitting [3–7]. In addition to experimental approaches, theoretical methods such as estimations based on surface energy calculations using density functional theory (DFT) [8,9], cohesive zone modelling [10–12], molecular dynamics simulations [13,14], and phase field modelling [15] have also been employed to predict fracture toughness. Nevertheless, experimental approaches remain essential for direct measurements at small scales as theoretical approaches often struggle to fully capture the complex mechanical responses, defect structures, or microstructural heterogeneities inherent to real material systems. The conventional nanoindentation approach has been widely used for measuring fracture toughness due to its versatility and ease of sample preparation [1, 16–18]; however, difficulties in determining crack geometry lead to measurement inaccuracies and limit its applications [5,19].

In contrast, the single cantilever beam geometry offers more accurate measurements and has become a preferred geometry for fracture toughness measurement of thin films or hard coatings [20–23]. Additionally, it enables site-specific testing, for instance targeting individual grains, phases, or interfaces within complex heterogeneous microstructures [24–28]. Fabrication of the single cantilever geometry predominantly relies on focused ion beam (FIB) techniques, which inherently introduce gallium ion-induced artefacts near the milled

This article is part of a special issue entitled: Nanomechanical Testing 2024 published in Materials Science & Engineering A.

* Corresponding author.
E-mail address: subin.lee@kit.edu (S. Lee).

https://doi.org/10.1016/j.msea.2025.148479
Received 4 April 2025; Received in revised form 5 May 2025; Accepted 9 May 2025
Available online 9 May 2025

notch. These artefacts include implanted ions at the notch that even change the stress state [25,29], chemical interaction and segregation along interfaces [30–32], and a finite notch root radius instead of an atomically sharp crack [25,33]. Such artefacts contribute to experimental uncertainties and critically limit the accuracy and reliability of fracture toughness (K_{IC}) measurement. Accurate K_{IC} values are essential for the reliable design and performance of micro-scale systems, such as microelectromechanical systems (MEMS), as well as thin films and hard coatings, where catastrophic mechanical failures can initiate from small defects or FIB-artefacts. Therefore, further refinement of experimental methods to minimize FIB-induced artefacts remains a pressing concern. Despite ongoing efforts, the complete elimination of these artefacts remains challenging, necessitating further refinement of micromechanical testing methods [34].

Additionally, the single cantilever beam is inherently prone to unstable crack growth, which implies that catastrophic failure occurs at the FIB milled notch surrounded by artefacts. Several alternative cantilever and notch geometries have been suggested over the years to overcome the aforementioned artefacts [6,35–40], each with limitations. One notable notching strategy is a modified through-thickness notch, also known as a bridge notch [3]. This notch is simply created by leaving thin material bridges on both ends of the cantilever's top surface (see Fig. 1). When the bridge notch meets specific geometrical criteria, the bridges experience higher stress intensities than the notch front under loading, causing them to fail before the notch front [3]. In the ideal case, as the stress intensity at the notch front right after the failure of the bridges is still below the critical value, the cracks from the bridges are arrested initiating the final fracture of the cantilever from the atomically sharp natural cracks upon further loading.

After the introduction of the bridge notch concept, Brinckmann et al. [41] employed finite element method (FEM) simulations to evaluate the stress intensity at the bridges in comparison to the ones at the notch front in through-thickness notch geometry. These calculations provided guidelines for designing bridge and notch geometries to ensure that cracks from the bridge failures are first arrested before the entire cantilever's catastrophic failure. However, experimental observation of crack arrest and bridge failure in the small scale fracture testing was not reported until the recent work of Zhang et al. [42]. In their study, crack arrest was observed experimentally in CrN/AlN and CrN micro cantilevers, where crack growth was arrested after the failure of material bridges, and the resulting natural cracks subsequently grew, leading to the final fracture of the cantilever.

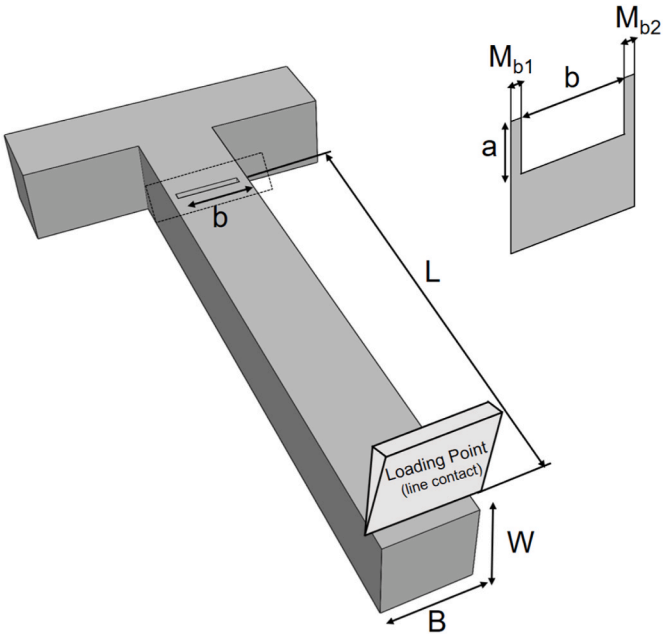

Fig. 1. Schematic drawing of the cantilever geometry showing the bridge notch with the designations of the geometry: *W*—cantilever thickness, *B*—cantilever width, *L*—cantilever length, *a*—notch depth, *b*—notch width, M_{b1} and M_{b2}—width of material bridges 1 and 2, respectively.

So far, bridge failure has only been experimentally observed in a specific bridge notch geometry [42]. However, it is essential to identify the range of bridge notch geometries likely to promote crack arrest. Therefore, a systematic investigation into the influence of varying notch and bridge geometries remains necessary. Such a study would not only provide experimental validation to complement the simulation work by Brinckmann et al. [41], but also address the source of overestimated fracture toughness of bridge-notched micro cantilevers in some material systems. As an example, previous studies have reported inconsistent mean values of fracture toughness, K_{IC}, for CrN coatings depending on the width of material bridges in the milled bridge notch. Rield et al. [23] and Best et al. [43] reported mean K_{IC} values of 3.8 ± 0.2 MPa $m^{0.5}$ and 3.4 ± 0.3 MPa $m^{0.5}$, respectively, for notches with wide material bridges. In contrast, a mean K_{IC} of 2.8 ± 0.2 MPa $m^{0.5}$ was measured by Zhang et al. [42] for narrow (thin) bridges, highlighting the sensitivity of measured fracture toughness to bridge geometry.

To address these gaps, this study investigates the influence of notch and bridge geometries on crack arrest using single crystalline silicon cantilevers. Silicon is chosen as a model material system due to its well-documented small-scale fracture behaviour [4,37,44,45] and the possibility of producing thousands of cantilevers using lithography. Approximately 1200 micro cantilevers with consistent dimensions were fabricated on a single piece of sample with a size of 20 × 20 mm using a lithography process, with 150 of these tested using *in situ* scanning electron microscope (SEM) fracture experiments. This fabrication method saves preparation time, enabling a statistically sound evaluation of notch geometry effects. Initially, micro-cantilevers were fabricated with varying notch depths while maintaining constant bridge widths. Subsequently, experiments were performed with varying bridge widths and fixed notch depths to systematically evaluate their influence on crack arrest behaviour.

2. Experimental procedure

2.1. Materials

A 100 mm diameter silicon on insulator (SOI) wafer (Siegert GMBH, Germany) was used as starting material to make test samples for the investigations. The wafer had a 3 μm-thick silicon device layer deposited on a 525 μm-thick silicon substrate separated by a 5 μm buried oxide (BOX) layer. The BOX layer acts as a barrier to isolate the device from the substrate, thereby preventing etching from progressing between the silicon layers and making it possible to fabricate MEMS devices and other similar structures [46,47]. The wafer was in the (110) normal orientation.

2.2. Cantilever preparation and notching

1200 micro cantilevers were produced at the Karlsruhe nano micro facility (KNMFi) using a combination of electron beam lithography and reactive ion etching. The as-received wafer was first spin-coated with polymethyl methacrylate (PMMA) (Labspin6, Süss MicroTec SE, Germany) electron beam resist to protect the surface from contamination during the subsequent cutting process. Then, the wafer was cut into 20 × 20 mm chips, and each chip was marked by a parallel line on the backside to identify its in-plane crystallographic orientation for subsequent steps.

The chip (hereafter called sample) was ultrasonically cleaned in acetone for 10 min, then rinsed in isopropanol and dried by nitrogen gas. A bi-layer of PMMA was then spin-coated on the sample, which resulted in a total resist layer thickness of 400 nm. Then, the pattern for the

cantilevers was exposed to the resist layers on the sample by electron beam (EPBG5200Z, Raith GmbH, Germany) equipped with Beamer (GenISys GmbH, Germany) pattern generator system at 100 kV with a dose of 900 μC/cm^2. In the next step, the exposed sample was developed in a 1:1 solution of Methyl isobutyl ketone and isopropanol (MIBK:IPA) solution for 45 s, followed by deposition of a 100 nm chromium film by electron beam evaporation (UNIVEX 400, Leybold GmbH, Germany). Finally, the PMMA resist layer was lifted off by dipping the sample in acetone for 5 min in a 50 % power ultrasonic bath. At the end of the lithography process, a hard chromium mask remains on the sample surface in preparation for etching. The steps for the electron beam lithography process are shown in Step 1 of Fig. 2.

Deep reactive ion etching (DRIE) of the sample with the chromium hard mask was done cryogenically in an inductively coupled plasma (ICP) lab system (100 ICP-RIE 380, Oxford Instruments, United Kingdom) (Step 2, Fig. 2). First, the sample was cooled to −95 °C in the chamber before the etching began. Then, etch gases, sulphur hexafluoride (SF_6), and oxygen were pumped into the chamber at 24 sccm and 6 sccm flow rates, respectively. The etching process used a radio frequency (RF) power of 8 W and an ICP power of 800 W at a chamber pressure of 5 mTorr and a strike step of 4 s, which resulted in an etching rate of 1 μm/min and a total etching time of 3 min and 30 s.

Subsequently, the sample was wet-etched to remove the BOX layer by immersing it in a 5 % buffered HF solution for 1 h, then rinsing it in isopropanol, which produced free-standing micro cantilevers on the SOI's device layer. Finally, the chromium mask was removed from the surface of the cantilever using TechniEtch Cr01 etchant (ceric ammonium nitrate: Perchloric acid: water = 10.9 %: 4.25 %: 84.85 %) for 2 min before rinsing off in ethanol (Step 3, Fig. 2). An array of the cantilevers produced by the steps described above is shown in Fig. 3.

These free-standing silicon cantilevers, which had nominal dimensions of 2–2.5 μm width and thickness and 10–12 μm length, were notched perpendicular to the silicon's (111) cleavage plane. Line elements were utilized to mill bridge notches (see Fig. 1) on the micro cantilevers using a Ga^+ FIB (Crossbeam 550L, Carl Zeiss AG, Germany) at an acceleration voltage of 30 kV with a beam current of 20 pA. The notch depths, a/W, varied from 0.20 to 0.45, and bridge width, 1-b/B, varied from 0.01 to 0.17. 150 cantilevers were tested within the framework of this study.

2.3. In situ SEM deformation testing

Micro cantilever fracture experiments were performed *in situ* in an SEM (Merlin, Carl Zeiss AG, Germany) using a PI 89 indenter (Hysitron, Bruker, USA) equipped with a 10 μm conductive diamond wedge tip (Synton-MDP AG, Switzerland). The sample was tilted at an angle of 15° using an in-house pre-tilt holder to increase the electron signal to the secondary electron detector. A low load displacement-controlled transducer with a maximum load of 10 mN and noise floor of 0.4 μN was used for all the experiments because the low noise of this transducer enhances the direct observation of bridge failure [42]. Displacement rates of 10 nm/s were used in the fracture tests.

3. Results

3.1. Fracture response via crack arrest

Representative mechanical testing data from a single micro cantilever experiment are shown in Fig. 4. Fig. 4a presents an SEM image of the test setup, which includes the notched cantilever and the wedge used for the experiments. The corresponding load-displacement curve shows an initially linear elastic response, as expected for single crystalline silicon, followed by two small load drops before the final fracture (Fig. 4b). No visible change is observed in the cantilever until point *c* (Fig. 4c). As loading progresses, a first a drop occurs at point *d,* which corresponds to fracture at the first bridge (red arrow in Fig. 4d), then a second drop is observed at point *e*, associated with the fracture of the second bridge (indicated by arrows in Fig. 4e), before the final fracture event at point *f*. The cross-sectional image (Fig. 4f) reveals a cleanly cleaved (111) fractured surface, indicating brittle fracture behaviour. Green arrows mark the broken bridges. These observations indicate the arrest of a growing crack in the bridge-notched silicon cantilevers similar to those reported for CrN/AlN multi-layers and CrN hard coatings by Zhang et al. [42]. After each test, the bridge width (1-b/B) is calculated from the notch width, *b*, measured in the middle of the fractured notch plane (see horizontal yellow line in Fig. 4f), while the notch depth is measured from the top of the cantilever to the notch front.

3.2. Effect of notch and bridge geometry on crack arrest

The apparent fracture toughness (K_{IQ}) is calculated from the load at the final fracture (point *f*, Fig. 4) under the assumption that bridge failure precedes final fracture and the shape of the notch before the final fracture is equivalent to a through-thickness notch using (Eqns. (1) and (2)) [3]:

$$K_{IQ} = \frac{F_C L}{BW^{3/2}} f_{Matoy}\left(\frac{a}{W}\right) \tag{1}$$

$$f_{Matoy}\left(\frac{a}{W}\right) = 1.46 + 24.36\left(\frac{a}{W}\right) - 47.21\left(\frac{a}{W}\right)^2 + 75.18\left(\frac{a}{W}\right)^3 \tag{2}$$

Here, F_C is the maximum load at fracture, and *L, B, W,* and *a* represent the geometry of the cantilever, as described in Fig. 1, and f_{Matoy} is a geometry correction factor.

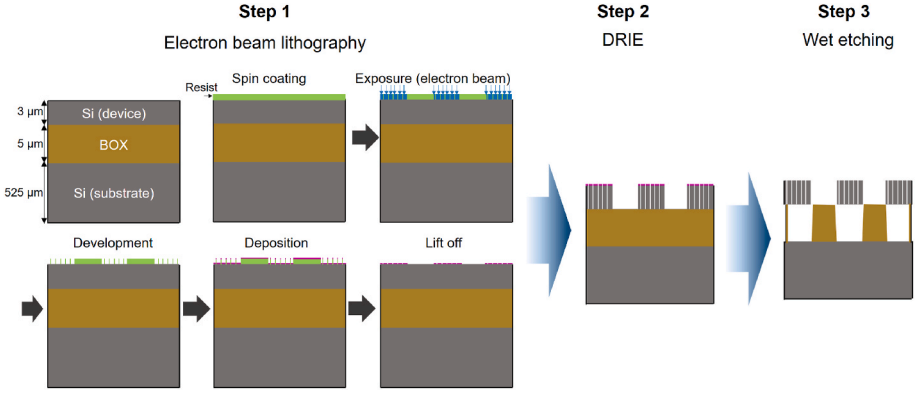

Fig. 2. Cross section of the cantilever fabrication steps on the SOI wafer. Step 1 summarizes the Electron beam lithography process used for metal (chromium) deposition on the surface of the silicon device layer. Steps 2 and 3 show the deep reactive etching and wet etching processes, respectively. (For interpretation of the references to colour in this figure legend, the reader is referred to the Web version of this article.)

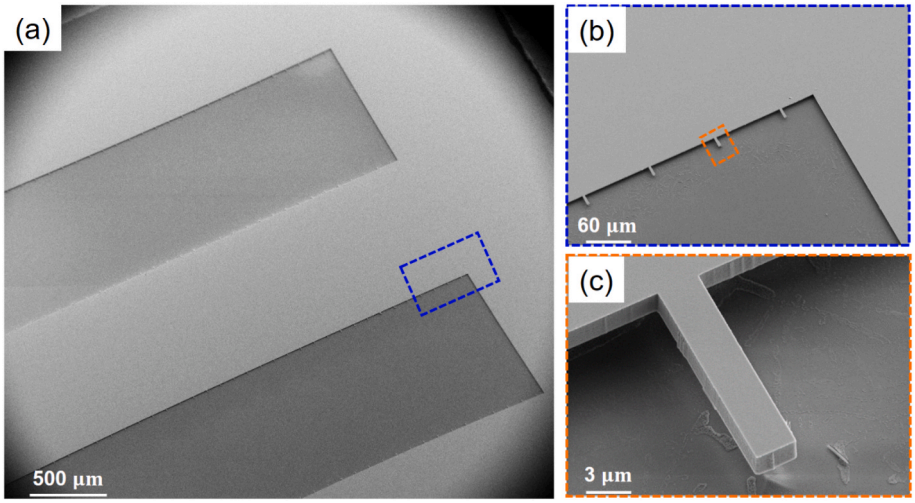

Fig. 3. SEM image of (a) section of 20 × 20 mm chip where the cantilevers were prepared, (b) a magnified view of one row in (a), showing cantilevers on the row, and (c) one cantilever produced from combined lithography and DRIE process.

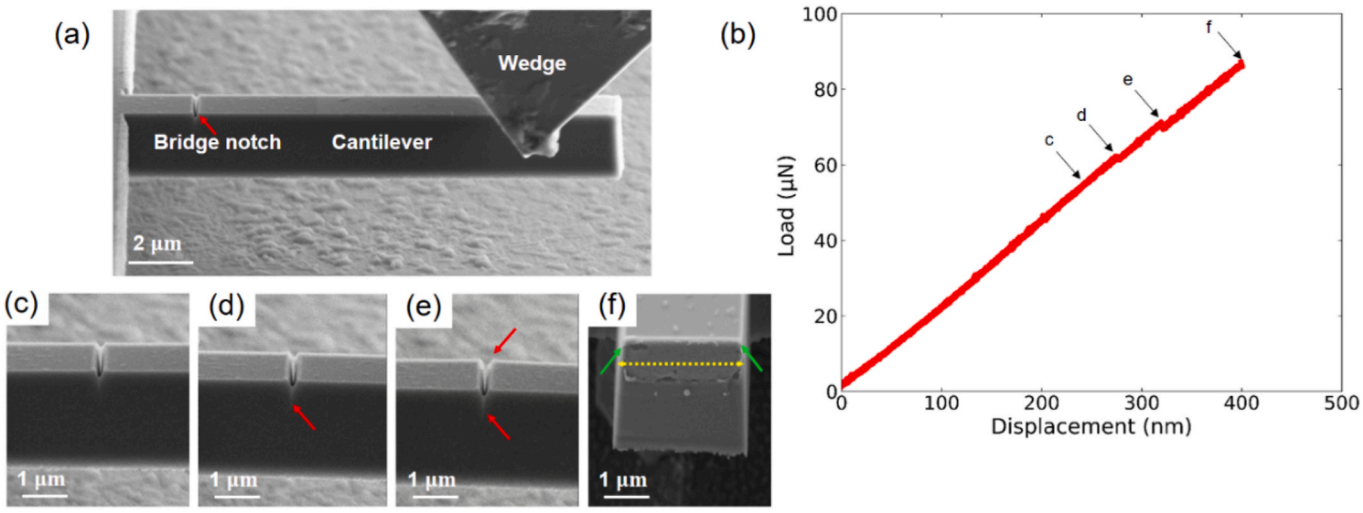

Fig. 4. (a) SEM image of the experiment's test setup. (b) Load-displacement curve from *in situ* SEM micro fracture tests of a silicon cantilever with a bridge notch. (c) SEM image of the cantilever at the start of the test, (d) after the failure of the first bridge, (e) after crack extension from the first bridge and failure of the second bridge—red arrows point to failed bridges in both images. (f) Cross-section of the cantilever after final fracture showing the geometry of the two bridges (green arrows) and the yellow line indicating the notch width. (For interpretation of the references to colour in this figure legend, the reader is referred to the Web version of this article.)

The calculated K_{IQ} values for all tested cantilevers are plotted in Fig. 5 as a function of bridge notch geometry, precisely the bridge width and notch depth. Filled circles in the plot indicate samples that showed bridge failure, evident from both *in situ* SEM images and load-displacement curves (load drops). Open circles, on the other hand, represent samples that did not show a load drop before final fracture. The through-thickness notch assumption in Eqn. (1) is valid for filled circles, where crack arrest and bridge failure are observed. For open circles, where no crack arrest is observed, this assumption is erroneous, as it remains unclear if the final fracture originates at the bridges or directly at the FIB notch front. For simplicity, the plot in Fig. 5 is segmented into four regions (I, II, III, and IV) representing different ranges of bridge notch geometries, and representative *postmortem* SEM images of the notch geometries are placed at the borders of the data plot. In addition, a section of the map applicable to displacement-controlled experiments from Ref. [41] is plotted on the experimental data represented as red lines marked *0.9*, *1.0,* and *1.1* to compare existing simulations and the present experiments.

A detailed look at the plot in Fig. 5 shows open circles in the lower-left corner, which means bridge failure and subsequent crack arrest are not observed before final failure in these cantilevers. In region I, where cantilevers have thin material bridges (1-b/B $<$ 0.1) and shallow notches ($a/W < 0.3$), the average K_{IQ} for samples is 1.01 ± 0.02 MPa $m^{0.5}$, comparable to the fracture toughness of single crystalline silicon previously reported in the literature (0.7–1.3 MPa $m^{0.5}$) [48].

Similarly, bridge failure is not observed in region II, where the cantilevers have comparable notch depth as region I ($a/W < 0.3$) but thicker bridges (1-b/B $\geq$ 0.1). In contrast to region I, the average K_{IQ} increases in this region (see Table 1 for values). This apparent increase in fracture toughness with increasing bridge width could be attributed to the relocation of the point of highest stress intensity in the cantilevers as the bridges get thicker.

Deeper notches show distinct behaviours in different regions of the plot. In region III, where cantilevers have a/W ratios between 0.3 and 0.4 and 1-b/B $<$ 0.1, crack arrest is observed as indicated by filled circles. The average K_{IQ} for these cantilevers is 1.09 ± 0.02 MPa $m^{0.5}$,

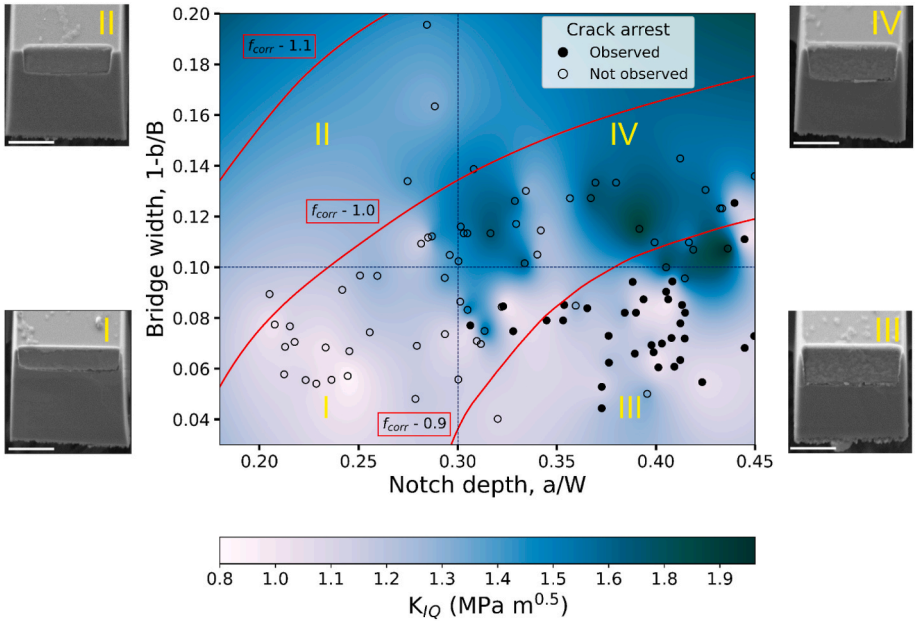

Fig. 5. K_{IQ} assuming through-thickness notch after bridge failures for samples with different bridge and notch geometries. Filled and unfilled circles represent observation and absence of crack arrest, respectively. Representative *postmortem* SEM images (scale bar is 1 μm) show the plot's bridge notch geometries in different regions (I, II, III, and IV). The red lines are stress intensity ratio (f_{corr}) lines extracted from existing simulation maps [41]. (For interpretation of the references to colour in this figure legend, the reader is referred to the Web version of this article.)

Table 1
Average fracture toughness and standard error of the mean measured from cantilevers with different notch depth and bridge width.

Region	Notch depth (a/W)	Bridge width (1-b/B)	Mean K_{IQ} (MPa m$^{0.5}$)	Width of K_{IQ} (Std. dev.)	Crack arrest
I	<0.3	<0.1	1.01 ± 0.02	0.08	No
II		≥0.1	1.32 ± 0.04	0.14	No
III	0.3–0.4	<0.1	1.09 ± 0.02	0.10	Yes
IV		≥0.1	1.48 ± 0.04	0.16	No

aligning closely with the expected fracture toughness of single crystalline silicon. In contrast, increasing the bridge width in region IV prevents crack arrest during experiments. This was accompanied by considerably higher toughness values – i.e., apparent toughening – (see Table 1), similar to the behaviour observed for shallow notches. Please note that the K_{IQ} values in Table 1 represent the mean value and the standard error of the mean.

Lastly, the experimental data is compared to the predictions for failure of material bridges from FEM simulations [41]. *0.9*, *1.0*, and *1.1* red lines in Fig. 5 denote the stress intensity ratio (f_{corr}) in micro cantilevers with bridge notches. f_{corr} is a bridge notch correction factor initially calculated for different bridge widths and notch depths by dividing the stress intensity factor at the notch front by the stress intensity at the top half of the bridge [41]. A ratio less than *1.0* signifies that the stress intensity at the bridges is higher than at the center of the notch, which would favour bridge failure and crack arrest. On the other hand, the stress intensity at the notch center is higher than at the bridges when the stress intensity ratio is greater than *1.0*, so that catastrophic failure of the cantilever is expected before observing bridge failures or crack arrest. Our results show that crack arrest occurs well-below the predicted *1.0* line in geometries with thin material bridges and deep notches. Instead, the cantilevers that showed crack arrest in the experimental data had bridge-notch geometries that fell below the *0.9* line. Possible reasons for this discrepancy will be addressed in subsequent sections.

Our experimental observations can be summarized into three points: (1) Thin bridges and deep notches lead to crack arrest before the final fracture from the natural crack, yielding K_{IQ} values that closely match the K_{IC} of silicon. (2) Thin bridges with shallow notches, while not exhibiting crack arrest, still show K_{IQ} values comparable to K_{IC}. (3) Thick bridges, regardless of notch depth, do not exhibit crack arrest, and their K_{IQ} values are significantly higher than K_{IC}, indicating apparent toughening effects.

In the absence of crack arrest, the toughness values are designated K_{IQ} which is geometry or system-dependent, particularly in the case of FIB-milled specimens, as the influence of bridge geometry on the observed results cannot be ignored. Later in the manuscript, further discussions will be made on the consequence of bridge width on fracture measurements of small samples.

4. Discussion

4.1. Possible origins of the discrepancy between experiments and simulations

In our experiment, crack arrest was only observed in a specific bridge notch geometry, i.e. for thin bridges and deep notches. All other bridge notch geometries did not show crack arrest during the tests. The absence of crack arrest is expected in bridge notch geometries with stress intensity ratios greater than *1.0* because the center of the FIB milled notch is the location of highest stress intensity [41]. However, some bridge notch geometries with stress intensity ratios less than *1.0* did not show crack arrest, specifically cantilevers with stress intensity ratios between *0.9* and *1.0*.

One probable reason for the absence of bridge failure in these bridge notch geometries is the deviation between the experimental and simulated sample geometries. The tapered material bridges in the experiment lead to less effective stress localization at the bridges, hence the absence of bridge failure. Imperfections in the bridge notch geometry from FIB milling, like redeposition or roundness of the inner corners of the material bridges, are also factors that distinguish experimental geometry from ideal geometry. These factors – the shape of the cantilever, the shape of the bridge, and roundness of inner corner of the bridge – which cannot be eliminated from FIB milled notches, contribute majorly to the

mismatch seen between the predictions of crack arrest in simulated and experimental geometries (Fig. 5).

Additionally, the tapered geometry introduces analysis uncertainties during *postmortem* SEM measurements of the bridge width. For instance, the bridge width can either be underestimated or overestimated depending on whether the measurement is taken from the top or bottom of the notch's *postmortem* SEM image, which could shift the data upwards or downwards when compared to the simulation reference. Bridge width measurements taken from the top of the notch cross section shifts the data to the bottom of Fig. 5, introducing further disparity between the predictions and the experiments (see Supplementary Fig. S1 for measurements from the top part of the bridge notch).

A final possible reason for the mismatch between both studies is the assumed intrinsic displacement-controlled loading conditions in the simulation, which deviate from the actual setup in commercially available indenter systems. The indenter used in our study is a displacement-controlled device with a 78 kHz feedback rate and a maximum data acquisition rate of 39 kHz, which could mean that low magnitude of load drops may not be captured in the load-displacement plots. Shallow notches (region I, Fig. 5) are particularly affected by our indenter's intrinsic mode of operation because, according to the simulations, the magnitude of the load drop is influenced by notch depth. Additionally, the compliance of the load cell may lead to a mixture of load and displacement-controlled behaviour of the system.

4.2. Consequence of bridge width on toughness measurements

To discuss the influence of bridge width on measured fracture toughness, we compare results obtained from cantilevers with thin and thick bridges at a fixed notch depth (a/W between 0.3 and 0.4) in a cumulative distribution plot (Fig. 6). K_{IC} represents data from cantilevers with thin bridge widths (1-b/B $<$ 0.1), which showed crack arrest. For the cantilevers with thick bridges (1-b/B $\geq$ 0.1) where crack arrest was absent, K_{IQ} is calculated assuming through-thickness notch assumptions. However, this assumption does not capture the geometry of a bridge-notched cantilever and, K_{IQ} needs to be corrected by f_{corr}. Therefore, a new fracture toughness value, $K_{IQ\_corrected}$, is calculated by modifying from Eqn. (1) by f_{corr} (Eqn. (3)):

$$K_{IQ\_corrected} = \frac{K_{IQ}}{f_{corr}} \tag{3}$$

The ability to correct the measured toughness for cases without bridge failure is analysed based on Fig. 6. While the values the fracture toughness in case of crack arrest is close to expected values for silicon, both, the uncorrected as well as corrected value for samples without crack arrest are far from literature values. Even more, f_{corr} is seen to shift K_{IQ} to higher toughness values, signifying that the correction factor cannot be applied to samples without observable crack arrest. Therefore, the observation of crack arrest is crucial to the success of bridge-notched micro cantilever fracture experiments. We recommend using material bridges thinner than 0.1 and notch depths between 0.3 and 0.4 to facilitate bridge failure and crack arrest in bridge-notched single cantilevers. This would correspond to 100 nm wide bridges on each side of the top surface of a 2-μm thick cantilever. Bridge failure can only be confirmed when it is indicated by load drops and observed in an *in situ* experimental setup. After both conditions are satisfied, through-thickness notch assumptions can be applied to extract valid fracture data from bridge-notched single cantilevers.

4.3. Fracture toughness of bridge-notched silicon cantilevers

The small plastic zone size of silicon makes it possible to obtain geometry-independent fracture toughness values from micro fracture experiments [33,44,50,51]. In silicon, the (111) plane, being the lowest resistant fracture plane [52], has reported fracture toughness between 0.65 and 1.0 MPa $m^{0.5}$ based on different measurement methods [53–56] at the bulk scale. Tanaka et al. [52] reported fracture toughness of 0.69 MPa $m^{0.5}$ from indentation tests, while 1.1 $\pm$ 0.02 MPa $m^{0.5}$ was

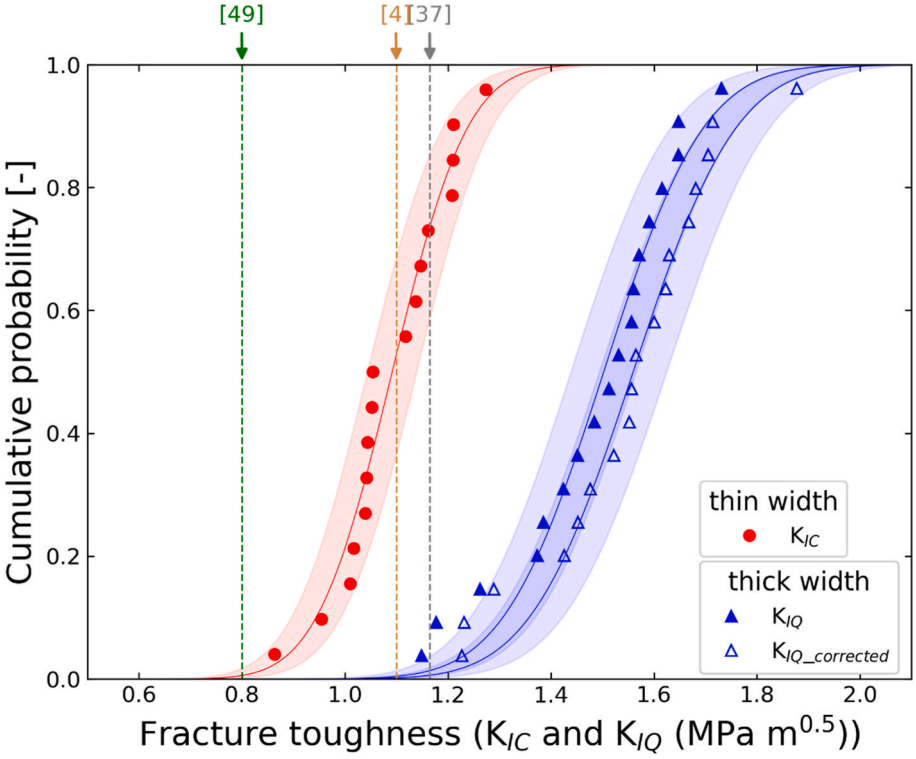

Fig. 6. Cumulative distribution of fracture toughness in silicon cantilevers with thin bridge widths where crack arrest occurred (K_{IC}) and thick bridge widths without crack arrest (K_{IQ} and $K_{IQ\_corrected}$) for cantilevers without crack arrest. Fracture toughness values of Si (111) measured from other micron scale studies are shown as vertical dashed lines in the plot [4,37,49]. (For interpretation of the references to colour in this figure legend, the reader is referred to the Web version of this article.)

reported from single cantilever-based studies by pentagonal beams [4] and triangular beams [37]. DelRio et al. [49] recently measured fracture toughness between 0.7 and 0.9 MPa $m^{0.5}$ for Si (111) in stable crack growth experiments using a double cantilever beam geometry. These literature values indicate a scatter in the fracture toughness of Si (111) measured using different geometries. In the bridge-notched cantilevers, the fracture toughness, K_{IC}, of Si (111) measured using thin bridges and deep notches is 1.1 ± 0.1 MPa $m^{0.5}$, which is within the reported range of for single crystalline silicon in both small and bulk scale studies. Additionally, our results align well with the theoretical predictions from an atomic-scale simple closed-form formula, where K_{IC} of Si (111) was calculated to be between 0.9 and 1.2 MPa $m^{0.5}$ [57,58], supporting the presence of an atomically sharp crack front after the failure of material bridges. These findings suggest that the bridge notch geometry could be used to obtain true material properties, provided that crack arrest precedes final failure.

5. Conclusion

This study systematically showed the region where bridge failure is expected in single crystalline silicon using *in situ* displacement-controlled cantilever bending experiments. The summary of the findings is as follows:

- Cantilevers with thin material bridges ($1–b/B < 0.1$) and deep notches ($a/W > 0.3$) showed crack arrest during *in situ* testing before final fracture. In these notches, the fracture toughness (K_{IC}) of 1.0 ± 0.2 MPa $m^{0.5}$ and 1.1 ± 0.1 MPa $m^{0.5}$ were calculated from the bridge and through-thickness notch, respectively.
- Crack arrest is absent in all cantilevers with shallow notches, $a/W < 0.3$, irrespective of bridge width. Also, cantilevers with thick bridges ($1–b/B > 0.1$) did not show crack arrest at all notch depths; apparent toughening effects were observed.
- A slight mismatch exists between the predicted bridge notch geometry for crack arrest and the experimental geometry. This disparity could be attributed to the experimental geometry's deviations from the ideal geometry and contributions from the commercial loading setup.
- Bridge notch correction factor, f_{corr}, is not sufficient to address the apparent toughening observed in notches with thick bridges. Hence, realistic fracture toughness values, K_{IC}, can only be obtained when crack arrest precedes final fracture in experiments with bridge notches.
- Thin bridges and deep notches are crucial for successful bridge-notched micro cantilever experiments, which results in fracture toughness values that are similar to theoretical predictions made on atomic-scale parameters.

CRediT authorship contribution statement

Eloho Okotete: Writing – review & editing, Writing – original draft, Methodology, Investigation, Formal analysis. **Alban Muslija:** Methodology, Investigation. **Judith K. Hohmann:** Methodology, Investigation. **Manfred Kohl:** Project administration, Methodology. **Steffen Brinckmann:** Formal analysis. **Subin Lee:** Writing – review & editing, Supervision, Methodology, Formal analysis, Conceptualization. **Christoph Kirchlechner:** Writing – review & editing, Supervision, Funding acquisition, Formal analysis, Conceptualization.

Declaration of competing interest

The authors declare that they have no known competing financial interests or personal relationships that could have appeared to influence the work reported in this paper.

Acknowledgement

Financial support from the Robert-Bosch-Foundation and from the Helmholtz Program Materials Systems Engineering is gratefully acknowledged. This work was partly carried out with the support of the Karlsruhe Nano Micro Facility (KNMFi, www.knmf.kit.edu), a Helmholtz Research Infrastructure at Karlsruhe Institute of Technology (KIT, www.kit.edu). C.K. kindly acknowledges the financial support by the German Research Foundation (DFG) [436506789].

Appendix A. Supplementary data

Supplementary data to this article can be found online at https://doi.org/10.1016/j.msea.2025.148479.

Data availability

Data will be made available on request.

References

[1] B. Lawn, R. Wilshaw, Indentation fracture: principles and applications, J. Mater. Sci. 10 (1975) 1049–1081, https://doi.org/10.1007/BF00823224.
[2] B.R. Lawn, D.B. Marshall, Indentation fractography: a measure of brittleness, J. Res. Natl. Bur. Stand. (United States). 89 (1984) 435–451, https://doi.org/10.6028/jres.089.024.
[3] K. Matoy, H. Schönherr, T. Detzel, T. Schöberl, R. Pippan, C. Motz, G. Dehm, A comparative micro-cantilever study of the mechanical behavior of silicon based passivation films, Thin Solid Films 518 (2009) 247–256, https://doi.org/10.1016/j.tsf.2009.07.143.
[4] D. Di Maio, S.G. Roberts, Measuring fracture toughness of coatings using focused-ion-beam-machined microbeams, J. Mater. Res. 20 (2005) 299–302, https://doi.org/10.1557/JMR.2005.0048.
[5] M. Sebastiani, K.E. Johanns, E.G. Herbert, F. Carassiti, G.M. Pharr, A novel pillar indentation splitting test for measuring fracture toughness of thin ceramic coatings, Philos. Mag. 95 (2015) 1928–1944, https://doi.org/10.1080/14786435.2014.913110.
[6] S. Liu, J.M. Wheeler, P.R. Howie, X.T. Zeng, J. Michler, W.J. Clegg, Measuring the fracture resistance of hard coatings, Appl. Phys. Lett. 102 (2013) 1–5, https://doi.org/10.1063/1.4803928.
[7] G. Sernicola, T. Giovannini, P. Patel, J.R. Kermode, D.S. Balint, T. Ben Britton, F. Giuliani, In situ stable crack growth at the micron scale, Nat. Commun. 8 (2017), https://doi.org/10.1038/s41467-017-00139-w.
[8] R. Perez, P. Gumbsch, AN AB initio study of the cleavage anisotropy in silicon, Acta Mater. 48 (2000) 4517–4530, https://doi.org/10.1007/s101560050020.
[9] A.A. Stekolnikov, J. Furthmüller, F. Bechstedt, Absolute surface energies of group-IV semiconductors: dependence on orientation and reconstruction, Phys. Rev. B Condens. Matter 65 (2002) 1–10, https://doi.org/10.1103/PhysRevB.65.115318.
[10] Rene de Borst, Numerical aspects of cohesive-zone models, Eng. Fract. Mech. 70 (2003) 1743–1757, https://doi.org/10.1016/S0013-7944(03)00122-X.
[11] J. Planas, M. Elices, J. G, the Cohesive Zone Model : Advantages , Limitations and Challenges, 2002, p. 69.
[12] N. Chandra, Evaluation of Interfacial Fracture Toughness Using Cohesive Zone Model, vol. 33, 2002, pp. 1433–1447.
[13] J.G. Swadener, M.I. Baskes, M. Nastasi, Molecular Dynamics Simulation of Brittle Fracture in Silicon, vol. 89, 2002, pp. 19–22, https://doi.org/10.1103/PhysRevLett.89.085503.
[14] T.P. Swiler, J.H. Simmons, A.C. Wright, Molecular Dynamics Study of Brittle Fracture in Silica Glass and Cristobalite, vol. 182, 1995, pp. 68–77.
[15] C. Kuhn, R. Müller, A continuum phase field model for fracture, Eng. Fract. Mech. 77 (2010) 3625–3634, https://doi.org/10.1016/j.engfracmech.2010.08.009.
[16] D.S. Harding, W.C. Oliver, G.M. Pharr, Cracking during nanoindentation and its use in the measurement of fracture toughness, Mater. Res. Soc. Symp. Proc. 356 (1995) 663–668, https://doi.org/10.1557/proc-356-663.
[17] J. il Jang, G.M. Pharr, Influence of indenter angle on cracking in Si and Ge during nanoindentation, Acta Mater. 56 (2008) 4458–4469, https://doi.org/10.1016/j.actamat.2008.05.005.
[18] P. Ostojic, R. McPherson, A review of indentation fracture theory: its development, principles and limitations, Int. J. Fract. 33 (1987) 297–312, https://doi.org/10.1007/BF00044418.
[19] K.E. Johanns, J.H. Lee, Y.F. Gao, G.M. Pharr, An evaluation of the advantages and limitations in simulating indentation cracking with cohesive zone finite elements, Model. Simulat. Mater. Sci. Eng. 22 (2014), https://doi.org/10.1088/0965-0393/22/1/015011.
[20] H. Gopalan, A. Marshal, M. Hans, D. Primetzhofer, N. Cautaerts, B. Breitbach, B. Völker, C. Kirchlechner, J.M. Schneider, G. Dehm, On the interplay between microstructure, residual stress and fracture toughness of (Hf-Nb-Ta-Zr)C multi-metal carbide hard coatings, Mater. Des. 224 (2022) 111323, https://doi.org/10.1016/j.matdes.2022.111323.

[21] B. Völker, B. Stelzer, S. Mráz, H. Rueß, R. Sahu, C. Kirchlechner, G. Dehm, J. M. Schneider, On the fracture behavior of Cr2AlC coatings, Mater. Des. 206 (2021), https://doi.org/10.1016/j.matdes.2021.109757.
[22] S. Massl, W. Thomma, J. Keckes, R. Pippan, Investigation of fracture properties of magnetron-sputtered TiN films by means of a FIB-based cantilever bending technique, Acta Mater. 57 (2009) 1768–1776, https://doi.org/10.1016/j.actamat.2008.12.018.
[23] A. Riedl, R. Daniel, M. Stefenelli, T. Schöberl, O. Kolednik, C. Mitterer, J. Keckes, A novel approach for determining fracture toughness of hard coatings on the micrometer scale, Scr. Mater. 67 (2012) 708–711, https://doi.org/10.1016/j.scriptamat.2012.06.034.
[24] F. Iqbal, J. Ast, M. Göken, K. Durst, In situ micro-cantilever tests to study fracture properties of NiAl single crystals, Acta Mater. 60 (2012) 1193–1200, https://doi.org/10.1016/j.actamat.2011.10.060.
[25] A.D. Norton, S. Falco, N. Young, J. Severs, R.I. Todd, Microcantilever investigation of fracture toughness and subcritical crack growth on the scale of the microstructure in Al2O3, J. Eur. Ceram. Soc. 35 (2015) 4521–4533, https://doi.org/10.1016/j.jeurceramsoc.2015.08.023.
[26] W. Luo, C. Kirchlechner, X. Fang, S. Brinckmann, G. Dehm, F. Stein, Influence of composition and crystal structure on the fracture toughness of NbCo2 Laves phase studied by micro-cantilever bending tests, Mater. Des. 145 (2018) 116–121, https://doi.org/10.1016/j.matdes.2018.02.045.
[27] C. Tian, C. Kirchlechner, The fracture toughness of martensite islands in dual-phase DP800 steel, J. Mater. Res. 36 (2021) 2495–2504, https://doi.org/10.1557/s43578-021-00150-4.
[28] S. Gabel, S. Giese, R.U. Webler, S. Neumeier, M. Göken, Microcantilever fracture tests of α-Cr containing NiAl bond coats, Adv. Eng. Mater. 24 (2022), https://doi.org/10.1002/adem.202101429.
[29] C.M. Lauener, L. Petho, M. Chen, Y. Xiao, J. Michler, J.M. Wheeler, Fracture of silicon: influence of rate, positioning accuracy, FIB machining, and elevated temperatures on toughness measured by pillar indentation splitting, Mater. Des. 142 (2018) 340–349, https://doi.org/10.1016/j.matdes.2018.01.015.
[30] R.C. Hugo, R.G. Hoagland, In-situ TEM observation of aluminum embrittlement by liquid gallium, Scr. Mater. 38 (1998) 523–529, https://doi.org/10.1016/S1359-6462(97)00464-8.
[31] B.A. Benson, R.G. Hoagland, Crack growth behavior of a high strength aluminum alloy during LME by gallium, Scripta Metall. 23 (1989) 1943–1948, https://doi.org/10.1016/0036-9748(89)90487-0.
[32] N. Tsutsui, H. Koizumi, Intergranular/transgranular fracture in the liquid metal embrittlement of polycrystalline embrittlement of polycrystalline zinc, Procedia Struct. Integr. 13 (2018) 849–854, https://doi.org/10.1016/j.prostr.2018.12.162.
[33] S. Wurster, C. Motz, R. Pippan, Characterization of the fracture toughness of micro-sized tungsten single crystal notched specimens, Philos. Mag. 92 (2012) 1803–1825, https://doi.org/10.1080/14786435.2012.658449.
[34] L. Borasi, A. Slagter, A. Mortensen, C. Kirchlechner, On the preparation and mechanical testing of nano to micron-scale specimens, Acta Mater. (2024) 120394, https://doi.org/10.1016/j.actamat.2024.120394.
[35] E. Okotete, S. Brinckmann, S. Lee, C. Kirchlechner, How to avoid FIB-milling artefacts in micro fracture? A new geometry for interface fracture, Mater. Des. 232 (2023) 112134, https://doi.org/10.1016/j.matdes.2023.112134.
[36] N. Jaya B, V. Jayaram, S.K. Biswas, A new method for fracture toughness determination of graded (Pt,Ni)Al bond coats by microbeam bend tests, Philos. Mag. 92 (2012) 3326–3345, https://doi.org/10.1080/14786435.2012.669068.
[37] M.G. Mueller, G. Žagar, A. Mortensen, Stable room-temperature micron-scale crack growth in single-crystalline silicon, J. Mater. Res. 32 (2017) 3617–3626, https://doi.org/10.1557/jmr.2017.238.
[38] M.G. Mueller, V. Pejchal, G. Žagar, A. Singh, M. Cantoni, A. Mortensen, Fracture toughness testing of nanocrystalline alumina and fused quartz using chevron-notched microbeams, Acta Mater. 86 (2015) 385–395, https://doi.org/10.1016/j.actamat.2014.12.016.
[39] F.Y. Cui, R.P. Vinci, A chevron-notched bowtie micro-beam bend test for fracture toughness measurement of brittle materials, Scr. Mater. 132 (2017) 53–57, https://doi.org/10.1016/j.scriptamat.2017.01.031.
[40] B.S. Li, T.J. Marrow, S.G. Roberts, D.E.J. Armstrong, Evaluation of fracture toughness measurements using Chevron-notched silicon and tungsten microcantilevers, Jom 71 (2019) 3378–3389, https://doi.org/10.1007/s11837-019-03696-1.
[41] S. Brinckmann, K. Matoy, C. Kirchlechner, G. Dehm, On the influence of microcantilever pre-crack geometries on the apparent fracture toughness of brittle materials, Acta Mater. 136 (2017) 281–287, https://doi.org/10.1016/j.actamat.2017.07.014.
[42] Y. Zhang, M. Bartosik, S. Brinckmann, S. Lee, C. Kirchlechner, Direct observation of crack arrest after bridge notch failure: a strategy to increase statistics and reduce FIB-artifacts in micro-cantilever testing, Mater. Des. 233 (2023) 112188, https://doi.org/10.1016/j.matdes.2023.112188.
[43] J.P. Best, J. Zechner, J.M. Wheeler, R. Schoeppner, M. Morstein, J. Michler, Small-scale fracture toughness of ceramic thin films: the effects of specimen geometry, ion beam notching and high temperature on chromium nitride toughness evaluation, Philos. Mag. 96 (2016) 3552–3569, https://doi.org/10.1080/14786435.2016.1223891.
[44] B.N. Jaya, C. Kirchlechner, G. Dehm, Can microscale fracture tests provide reliable fracture toughness values? A case study in silicon, J. Mater. Res. 30 (2015) 686–698, https://doi.org/10.1557/jmr.2015.2.
[45] C.M. Lauener, L. Petho, M. Chen, Y. Xiao, J. Michler, J.M. Wheeler, Fracture of Silicon: influence of rate, positioning accuracy, FIB machining, and elevated temperatures on toughness measured by pillar indentation splitting, Mater. Des. 142 (2018) 340–349, https://doi.org/10.1016/j.matdes.2018.01.015.
[46] T. Kim, J. Lee, Fabrication and characterization of silicon-on-insulator wafers, Micro Nano Syst. Lett. 11 (2023), https://doi.org/10.1186/s40486-023-00181-y.
[47] L. Haobing, F. Chollet, Layout controlled one-step dry etch and release of MEMS using deep RIE on SOI wafer, J. Microelectromech. Syst. 15 (2006) 541–547, https://doi.org/10.1109/JMEMS.2006.876660.
[48] R.O. Ritchie, Failure of silicon: crack formation and propagation, in: 13th Work. Crytsalline Sol. Cell Mater. Process. Vail Color, 2003.
[49] F.W. DelRio, S.J. Grutzik, W.M. Mook, S.M. Dickens, P.G. Kotula, E.D. Hintsala, D. D. Stauffer, B.L. Boyce, Eliciting stable nanoscale fracture in single-crystal silicon, Mater. Res. Lett. 10 (2022) 728–735, https://doi.org/10.1080/21663831.2022.2088251.
[50] R. Pippan, S. Wurster, D. Kiener, Fracture mechanics of micro samples: fundamental considerations, Mater. Des. 159 (2018) 252–267, https://doi.org/10.1016/j.matdes.2018.09.004.
[51] T.L. Anderson, Fracture Mechanics, Third, CRC Press, 2005, https://doi.org/10.1201/9781420058215.
[52] M. Tanaka, K. Higashida, H. Nakashima, H. Takagi, M. Fujiwara, Orientation dependence of fracture toughness measured by indentation methods and its relation to surface energy in single crystal silicon, Int. J. Fract. 139 (2006) 383–394, https://doi.org/10.1007/s10704-006-0021-7.
[53] F.W. DelRio, R.F. Cook, B.L. Boyce, Fracture strength of micro- and nano-scale silicon components, Appl. Phys. Rev. 2 (2015), https://doi.org/10.1063/1.4919540.
[54] M. Brede, P. Haasen, The brittle-to-ductile transition in doped silicon as a model substance, Acta Metall. 36 (1988) 2003–2018, https://doi.org/10.1016/0001-6160(88)90302-1.
[55] C. St John, The brittle-to-ductile transition in pre-cleaved silicon single crystals, Philos. Mag. 32 (1975) 1193–1212, https://doi.org/10.1080/14786437508228099.
[56] R.J. Jaccodine, Surface energy of germanium and silicon, J. Electrochem. Soc. 110 (1963) 524, https://doi.org/10.1149/1.2425806.
[57] X. Hu, Y. Mai, Re -interpretation of the Weibull strength distribution of polycrystalline ceramics – characteristic strength and fracture toughness, J. Mech. Phys. Solid. 196 (2025) 106021, https://doi.org/10.1016/j.jmps.2024.106021.
[58] X. Hu, Q. Li, Z. Wu, S. Yang, Modelling fracture process zone width and length for quasi-brittle fracture of rock , concrete and ceramics, Eng. Fract. Mech. 259 (2022) 108158, https://doi.org/10.1016/j.engfracmech.2021.108158.